JOURNAL OF AIRCRAFT
Vol. 31, No. 2, March–April 1994

Computational Analysis of a Single Jet Impingement Ground Effect Lift Loss

Xin Zhang*
Southampton University, Southampton S09 5NH, England, United Kingdom
and
Dan N. Ing†
Logico Systems, Ltd., Surrey KT24 5AB, England, United Kingdom

A study was carried out on single round jet ground effect lift loss. The jet exit Mach number and velocity were 0.71 and 240 m/s, respectively. The effects of ground height, baffle plate edge, and jet exit turbulent intensity were assessed, and Navier-Stokes equations were solved using computational fluid dynamics. Turbulence closure was achieved using a k-ε model, and the result compared with calculations obtained with a differential stress model. Three baffle plate edges were tested (rounded, squared, and chamfered), and the ground heights varied from $\eta = 0.15$ to 0.8. It was found that flow mechanisms varied significantly with ground heights. A coherent vortex existed between the baffle plate and the ground at the low ground heights ($\eta < 0.25$), which suppressed and/or delayed separation at the baffle plate edge and induced high lift loss. At the high ground heights ($\eta \geq 0.25$), the vortex disappeared and separation at the plate edge played an important part in determining the lift loss. The baffle plate edge was found to account for as much as 14% of the ground effect lift loss. The stress model was found to improve the accuracy of the prediction.

Nomenclature

C_f = skin friction coefficient on baffle plate, $2 \cdot \tau/q$
C_p = specific heat
C_x = lift loss coefficient, $(G - G_\infty)/T_j$
D = baffle plate diameter
d = jet diameter
G = lift loss
H = ground height
k = turbulence kinetic energy
p = dynamic pressure
q = $\rho_j V_j^2$
T = temperature
T_j = jet thrust
t = time
V = flow velocity in vector form
V_j = jet exit velocity
x, y = cylindrical coordinates
ε = turbulence dissipation rate
ζ = bulk viscosity
η = nondimensional ground height, $H/(D - d)$
λ = thermal conductivity
ρ = density
σ_t = turbulent Prandtl number, 0.9
τ = shear stress
ψ = stream function

Subscripts
j = jet exit condition
∞ = out-of-ground condition

Received Aug. 6, 1992; revision received Nov. 30, 1992; accepted for publication Dec. 4, 1992; presented as Paper 93-0869 at the AIAA 31st Aerospace Science Meeting, Reno, NV, Jan. 11–14, 1993.

*Lecturer, Department of Aeronautics and Astronautics. Member AIAA.
†Director.

Introduction

Background

A SINGLE jet impinging on the ground induces lift loss and other adverse effects. An accurate prediction of the induced lift loss due to ground effect is required to make a realistic estimate of V/STOL aircraft performance. Over the past 30 yr, a number of experimental studies have been carried out to investigate the induced lift loss from an idealized test configuration of a baffle plate surrounding a single jet.[1–9] In Fig. 1, a sketch of the flow and coordinates system is given. A close examination of the published literature shows that considerable discrepancies exist among the lift loss data (Fig. 2). These exist despite the fact that many of the experiments were carried out with "similar" test configurations. It is suggested that these anomalies could be due to the slight variations in the experimental arrangements.[10]

The flowfield generated by a V/STOL aircraft includes both jet/crossflow interactions and jet impingements. Computational analyses of jets in crossflow have been carried out by a number of researchers.[11,12] In the present study, some features of a single jet impingement are analyzed. The effects of baffle plate edge, ground height, and jet exit characteristics are assessed. The discrepancies among the various investigations are highlighted and the possible causes identified. A flow model is established based on computational fluid dynamics by solving mass, momentum, and energy equations governing the compressible airflow. The study focuses on the correct setup of the flow and particularly the effects of baffle plate edge configuration.

Flowfield

Figure 1 depicts the flow patterns between a circular baffle plate and the ground, from the flow visualization carried out by Wyatt.[1] This represents an idealized flow often used in experimental studies. According to Wyatt,[1] at $H/D > 0.3$, pure in- and outflow were observed near the plate and the ground, respectively. At $H/D = 0.194$, the free boundary of the jet was attached to the outer portion of the plate, and a circulatory flow region was developed beneath the inner portion of the plate. At $H/D = 0.083$, the "attachment line" on the plate separating the region of in- and outflow moved

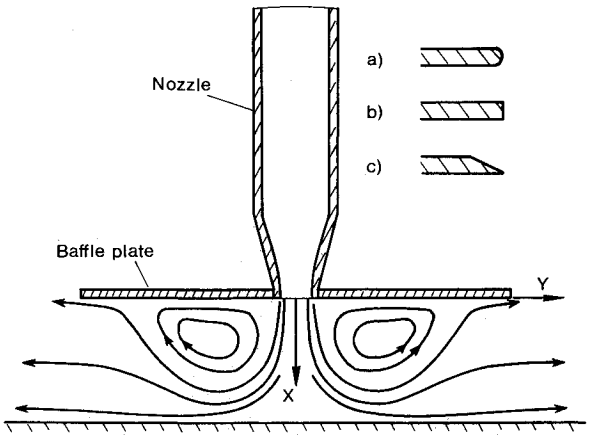

Fig. 1 Schematic of the flow: a) rounded edge, b) squared edge, and c) 26.57-deg chamfered edge.

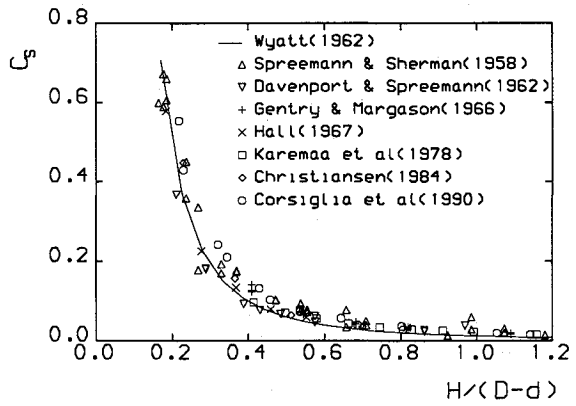

Fig. 2 Ground effect induced lift loss.

inwards, and the jet boundary layer separated from the ground. The rapid rise in ground suction as H/D was reduced appeared to be associated with the formation of the circulatory flow beneath the plate.

In the above description by Wyatt,[1] separation around the sharp edge of the baffle plate was not mentioned at $H/D \geq 0.3$. Evidence from smoke visualization by Mayson et al.,[13] however, indicates the presence of a standing ring vortex beneath the outer portion of the plate.

Experimental Data

Among the various experimental studies, Wyatt[4] and Corsiglia et al.[9] appear to be well executed and documented. It is therefore more likely that the discrepancies between the two data sets are due to real flow effects rather than errors in the data sets. Wyatt's[4] data were found to be among the lowest values of lift loss, while in contrast the data of Spreemann and Sherman[2] and Corsiglia et al.[9] exhibited the highest lift loss values.

Wyatt[4] data collapse well into a curve given by

$$C_s = 0.012\eta^{-2.3} \tag{1}$$

In Fig. 2, the variables are defined following those in the Wyatt[4] experiment. Only selected conditions from the original publications were used. Those selected enable meaningful comparisons to be drawn between the data sets. Attention is focused on the middle range of η, e.g., between 0.2–0.7, which is of practical interest and where the measurement accuracy is thought to be highest. These results correlate to within ±15–20% about the mean over the scatter band. The data sets can be loosely arranged together in order of agreement with Wyatt.[4] The best comparison is found in the experiments of Karemaa et al.[7] and Hall,[6] with agreement generally within a few percent. The second group comprises data from Davenport and Spreemann,[3] Gentry and Margason,[5] and Christiansen.[8] The agreement here is generally within 10–15%. The third group consists of Spreemann and Sherman[2] and Corsiglia et al.,[9] where discrepancies in the middle range of η are in the region of 20–30%, but in the case of Spreemann and Sherman,[2] improve as η reduces. A detailed discussion of these results is given by Ing and Bailey.[10]

Although it is debatable which are the primary and secondary causes for the discrepancies between the data sets, substantial emphasis has been placed in 1) jet exit flow characteristics/plenum chamber design; 2) nozzle/plate gap size and nozzle thickness at the jet exit; 3) baffle plate edge design; 4) ground plate design; 5) induced lift measurement; 6) test room size; 7) plenum blockage; and 8) jet pressure ratio. Turbulent intensity may also be of importance.[14] Parameters that researchers have generally found to have little effect on the lift loss forces are temperature, jet Reynolds number, and Mach number (in the subsonic range).

It is suspected that the induced flowfield surrounding the baffle plate, combined with the exponential variation of the induced lift with ground height, may be highly sensitive to small variations in test rig geometry, such as baffle plate edge design and exhaust flow characteristics. In fact, the test conducted by Mayson et al.[13] indicated the importance of plate edge design on the induced lift loss. This may explain to some extent the large discrepancies between Spreemann and Sherman[2] and Davenport and Spreemann,[3] using squared-edge and round-edge baffle plates, respectively. However, flow visualization from Wyatt[1] shows that the edge design may be less significant at low ground heights, $\eta \leq 0.2$, where outflow is present at the outer region of the baffle plate. This may also account for the generally improved correlation between the data sets at low ground heights.

Present Flow Conditions

In the present study, flowfields of jet/ground impingement with a baffle plate are investigated using computational fluid dynamics. The study first sets out to establish a flow model with the correct grid density and boundary conditions. This was followed by an investigation of the baffle plate edge effect. Three typical edge configurations were used: 1) a baseline configuration with a rounded edge, 2) a squared edge, and 3) a chamfered edge (Fig. 1).

The nozzle used is a BAe Warton model RA78-50 mm calibration nozzle.[10] d is 50 mm and D 500 mm. H varies from $\eta = 0.15$ to 0.8. Attention is focused on the middle ground height range between 0.2–0.3 as this is the most sensitive range where the flow mechanism changes. The baffle plate thickness is 8 mm. Jet Mach number is 0.71, V_j 240 m/s, ρ_j 1.262, and pressure ratio P_r 1.4. An unheated jet is used. The jet exit turbulence kinetic energy level is set at $0.002V_j^2$, and varied from $0.002V_j^2$ to $0.1V_j^2$ in the parametric study of the exit conditions.

Results are presented in the forms of velocity V/V_j, ψ, k, pressure coefficient p/q, C_f, and C_s.

Numerical Model

Governing Equations

The basic equations used to describe the flow comprise equations for conservation of mass, momentum, and energy. Density is calculated from the state equation. Turbulence is simulated by a standard k-ε model.[15] The governing equations in vector form can be written as

$$\frac{\partial \rho}{\partial t} + \nabla \cdot (\rho V) = 0 \tag{2}$$

$$\frac{\partial \rho V}{\partial t} + \nabla\cdot(\rho V \otimes V) - \nabla\cdot(\mu \nabla V) = -\nabla\left[p + \frac{2}{3}\rho k + \left(\frac{2}{3}\mu - \zeta\right)\nabla\cdot V\right] + \nabla\cdot[\mu(\nabla V)^T] \quad (3)$$

$$\frac{\partial \rho T}{\partial t} + \nabla\cdot(\rho V T) - \nabla\cdot\left[\left(\frac{\mu_t}{\sigma_t} + \frac{\lambda}{C_p}\right)\nabla T\right] = \frac{\partial p}{\partial t} \quad (4)$$

where the tensor product is defined as $(\boldsymbol{A} \otimes \boldsymbol{B})_{ij} = A_i B_j$. μ is the effective viscosity which is defined by

$$\mu = \mu_l + \mu_t$$

where μ_l is the molecular viscosity and μ_t the turbulent viscosity.

Density is calculated from the state equation

$$p = \rho R T \quad (5)$$

where $R = 287$.

In the k-ε model, μ_t is given as

$$\mu_t = C_\mu \rho (k^2/\varepsilon) \quad (6)$$

The transport equations for k and ε are

$$\frac{\partial \rho k}{\partial t} + \nabla\cdot(\rho V k) - \nabla\cdot\left[\left(\mu + \frac{\mu_t}{\sigma_k}\right)\nabla k\right] = P - \rho\varepsilon \quad (7)$$

$$\frac{\partial \rho \varepsilon}{\partial t} + \nabla\cdot(\rho V \varepsilon) - \nabla\cdot\left[\left(\mu + \frac{\mu_t}{\sigma_e}\right)\nabla \varepsilon\right] = C_1 \frac{\varepsilon}{k} P - C_2 \rho \frac{\varepsilon^2}{k} \quad (8)$$

where C_μ, C_1, C_2, σ_k, and σ_e are empirical constants and are given values of 0.09, 1.44, 1.92, 1.0, and 1.3, respectively. P is the shear stress production defined by

$$P = \mu \nabla V\cdot[\nabla V + (\nabla V)^T] - \tfrac{2}{3}\nabla\cdot V(\mu \nabla\cdot V + \rho k) \quad (9)$$

It is generally realized that the k-ε model overpredicts the spread rate of the jet. The present flow also undergoes large curvature changes. However, this study focuses on the flow around the baffle plate, not the wall jet and the fountain flow. In Vasquez-Malebran and Ing,[16] the ground pressure and the maximum velocity in the wall jet are predicted by a k-ε model and an algebraic stress model. The results differ only marginally. Those parameters set the overall conditions of the induced flow. As the present is mainly a parametric study, the use of the k-ε model is believed to be justified. When the differential stress model is used, the eddy-viscosity hypothesis is not invoked. Instead, equations for the individual Reynolds stress components are used. The momentum and stress equations are given in vector form by Clarke and Wilkes[17] and will not be repeated here.

Numerical Approach

The coordinate system is shown in Fig. 1, where the positive x axis is in the jet direction and the y axis along the flat baffle plate. The flow is axisymmetrical to the x axis. The center of the jet exit is located at the origin of the coordinate system. The physical space is divided into control volumes using nonstaggered grids. The grids that are used vary according to the ground height, ranging from 103 × 100 to 124 × 100. The largest grid covers −1000 to 360 mm in the x direction and 0 to 1000 mm in the y direction. They were chosen after the effect of grid density was tested. At Mach 0.71, a coarse grid of 88 × 88 gives a lift loss coefficient of 2.67 for the squared edge configuration at $\eta = 0.3$. The lift loss coefficient gradually approaches 0.278 as the local grid is refined. The 103 × 100 grid was chosen after the local grid refinement indicated acceptable changes. A typical grid is shown in Fig. 3.

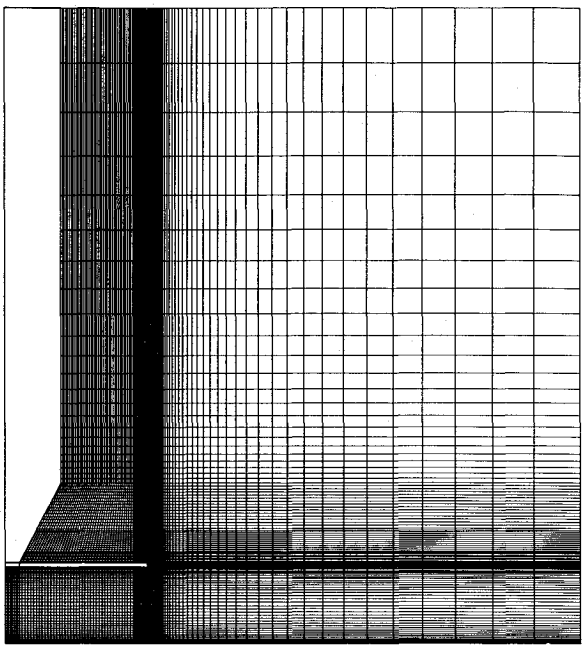

Fig. 3 Typical grid around the squared edge baffle plate.

On the ground and the baffle plate, the velocity is set to zero. In the near wall region, variables such as velocity are calculated by the classic linear-logarithmic wall-functions so that an exceedingly fine grid is not needed. Pressure condition is used for the upstream boundary and the pressure is fixed during the computation. Away from the baffle plate in the y direction, derivatives of the variables normal to the boundary are set to zero. Velocity components normal to the boundary are adjusted for mass conservation. The out-of-ground lift loss is calculated by moving the ground height to $H = 27d$ and setting derivatives of the variables normal to the ground to zero.

On the jet exit surface, the jet velocity is specified and fixed throughout the computation. k and ε are approximated respectively as

High Ground Height $\eta \geq 0.25$

As the ground height increases, the wall boundary layer detaches from the plate and the flow characteristics change accordingly. At $\eta = 0.2$, the vortex is still present between the ground and the plate. At higher ground heights, the vortex disappears and new flow features appear. The velocity field is now dominated by the entrainment to the wall jet and the induced flow around the baffle plate edge. Separation does occur at the edge of the plate. The velocity contour, streamlines, and turbulence kinetic energy contour at $\eta = 0.3$ are given in Figs. 7a–7c. Figure 7a shows the forming of the wall jet on the ground. Flow entrainment is indicated by the streamlines in Fig. 7b, though there is not a recirculating region between the ground and the plate. The absence of this mechanism will have significant implications in pressure field and lift loss, as shown later. The edge of the wall boundary layer can be seen in the turbulence kinetic energy distribution, which is now totally detached from the plate.

Results and Discussion

Induced Flowfields

It has been observed in flow visualization[1] that when H changes, the flowfield undergoes important changes. The vorticity, pressure fields, and the lift loss vary according to the ground height. In this study it is observed that while the flow characteristics remain largely the same at $\eta \geq 0.25$, they differ significantly at lower ground heights.

Low Ground Height $\eta < 0.25$

Separation is not observed at the edge of the plate at a low ground height of $\eta = 0.15$, or for the other two edge configurations (see later on the skin friction distribution). A vortex is formed between the outer portion of the plate and the ground (Fig. 4). This vortex is the product of outflow on the ground and induced flow around the edge of the plate. This ground height is critical in that the outer part of the wall jet on the ground is attached to the plate. This feature can be seen in Figs. 5a–5c, where the velocity contour, streamlines, and turbulence kinetic energy contour are presented. The induced vortex between the plate and the ground is clearly shown in the streamline plot. Also shown is the flow entrainment induced by the jet. The interaction between the wall jet and the plate is indicated by the turbulence kinetic energy contour plot. This feature disappears as the ground height increases. Around the edge of the plate, there is an adverse pressure gradient along the lower surface of the plate towards the jet exit (see the following discussion). However, it is apparently not severe enough to cause separation.

The lift loss is measured by the pressure distribution on the upper and lower surfaces of the baffle plate. In Fig. 6, the surface pressure distributions on both surfaces of the squared edge plate are presented. The pressure distribution on the upper surface is seen to contribute little to the lift loss. This feature is repeated for all the ground heights studied. On the lower surface, the predominant feature is not the pressure recovery along the plate, but the induced pressure distribution due to the vortex (Fig. 4). The significance of this vortex is that it appears below the outer portion of the plate, its effect is therefore significant. Apart from inducing a low-pressure distribution on the plate, the formation of the vortex also contributes to the suppression of the impending separation around the edge of the plate. In Fig. 6, the pressure distribution near the edge on the lower surface of the plate indicates an adverse pressure gradient to the jet exit. This is quickly overtaken by the pressure distribution induced by the vortex. This favorable pressure distribution suppresses, or even forces, the already separated flow to reattach. At the beginning of this study, it was surmised that the edge induced separation would play an important part in the induced pressure field between the ground and the plate. This would account for part of the large discrepancies between the various experimental data sets. With the presence of the vortex, this effect will be reduced as well.

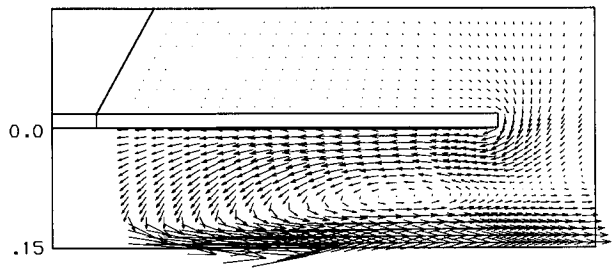

Fig. 4 Velocity vector at $\eta = 0.15$; square edge.

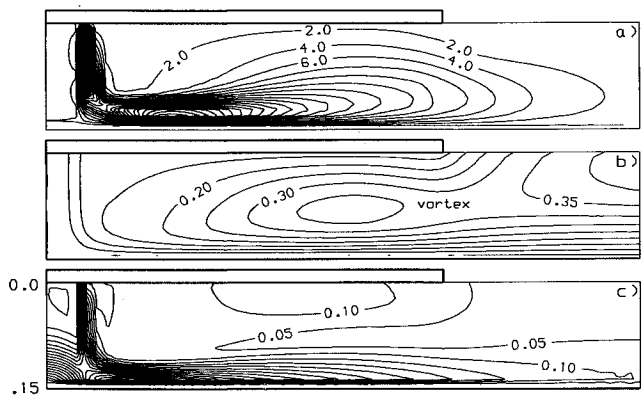

Fig. 5 Flowfields at $\eta = 0.15$: a) turbulence kinetic energy, $10^3k/V_j^2$; b) streamline, $\psi/(\rho_j V_j d^2)$; and c) velocity contour, V/V_j.

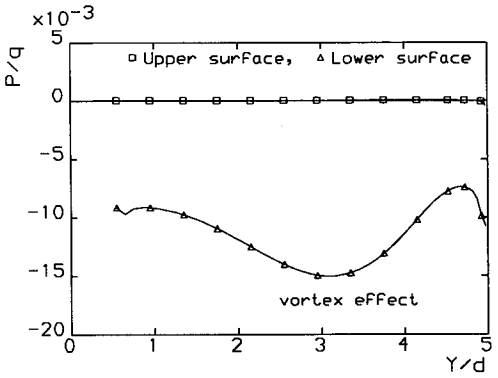

Fig. 6 Pressure distributions at $\eta = 0.15$; square edge.

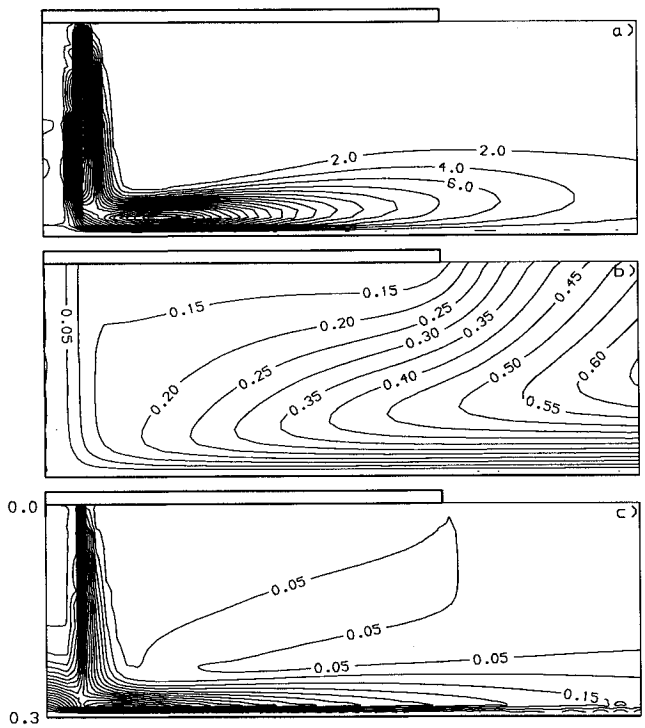

Fig. 7 Flowfields at $\eta = 0.3$: a) turbulence kinetic energy, $10^3k/V_j^2$; b) streamline, $\psi/(\rho_j V_j d^2)$; and c) velocity contour, V/V_j.

High Ground Height $\eta \geq 0.25$

As the ground height increases, the wall boundary layer detaches from the plate and the flow characteristics change accordingly. At $\eta = 0.2$, the vortex is still present between the ground and the plate. At higher ground heights, the vortex disappears and new flow features appear. The velocity field is now dominated by the entrainment to the wall jet and the induced flow around the baffle plate edge. Separation does occur at the edge of the plate. The velocity contour, streamlines, and turbulence kinetic energy contour at $\eta = 0.3$ are given in Figs. 7a–7c. Figure 7a shows the forming of the wall jet on the ground. Flow entrainment is indicated by the streamlines in Fig. 7b, though there is not a recirculating region between the ground and the plate. The absence of this mechanism will have significant implications in pressure field and lift loss, as shown later. The edge of the wall boundary layer can be seen in the turbulence kinetic energy distribution, which is now totally detached from the plate.

At the high ground heights, the pressure field on the upper surface also contributes little to the overall lift loss, and the loss is primarily due to the suction force on the lower surface (Fig. 11). Near the jet exit, the pressure drops due to the flow entrainment of the jet. The contribution of this part of the pressure distribution is not substantial. Around the edge of the baffle plate, the pressure drops sharply and then gradually recovers. This results in an adverse pressure gradient towards the jet exit and flow separation. As the coherent vortex is not present between the ground and the plate to alleviate the adverse pressure gradient, the separation will persist and increase in extent. The pressure distribution is now strongly influenced by the separation at the edge of the plate. Here, the edge configuration is very important. A stronger induced separation would mean higher pressure loss and, in turn, higher lift loss. As this effect occurs near the edge of the plate, its contribution to the lift loss is much more substantial. The existence of a separation region near the edge is confirmed by the skin friction (Fig. 8). The skin friction coefficient changes sign near the edge of the plate.

Although Wyatt[1] did not mention separation at $H/D \geq 0.2$, Mayson et al.[13] did notice a standing ring underneath the plate. This is caused by the separation, and can be seen more clearly in Fig. 9 at a high ground height of $\eta \geq 0.4$. The separation forms a large recirculating region underneath the plate near the edge.

Effect of Ground Height

In Fig. 10 the prediced lift loss coefficient is presented together with the experimental data. The predicted lift loss coefficient is seen to fall into the upper band of the experimental data. Comparison with Corsiglia et al.[9] is encouraging. The exponential rise of the lift loss coefficient as the ground height decreases below $\eta = 0.3$ is predicted. The gradual variation of the lift loss at $\eta \geq 0.6$ is also well predicted.

The change of flow mechanism as the ground height was increased to above $\eta \geq 0.3$ was discussed previously. The disappearance of the coherent vortex allows the separation

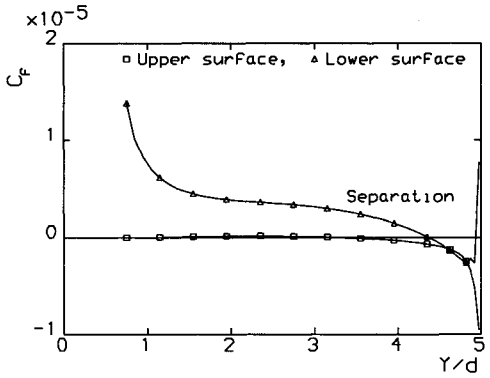

Fig. 8 Skin friction coefficient at $\eta = 0.3$; squared edge.

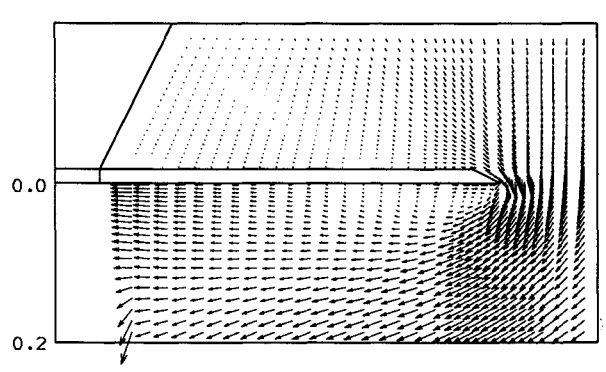

Fig. 9 Velocity vector at $\eta = 0.4$; chamfered edge.

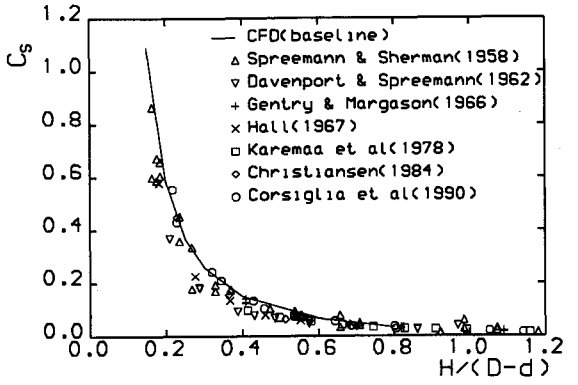

Fig. 10 Lift loss prediction.

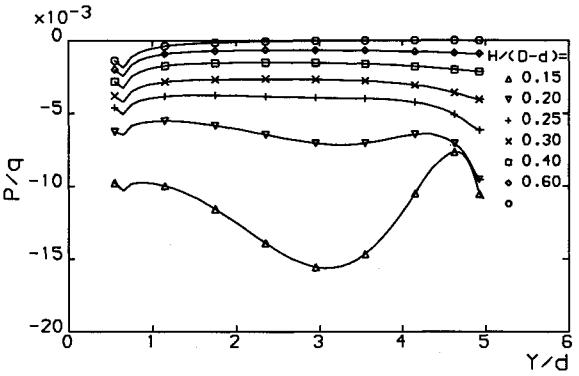

Fig. 11 Ground effects on the lower surface pressure; chamfered edge.

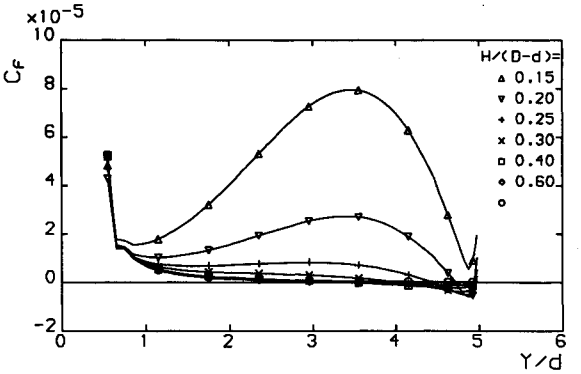

Fig. 12 Ground effects on the lower surface skin friction; chamfered edge.

on the edge to persist and reduces the pressure loss on the lower surface of the baffle plate. This change is clearly visible in Figs. 11 and 12, where the surface pressure and skin friction coefficient distributions on the lower of the chamfered edge baffle plate are given at various ground heights studied. In Fig. 11 the vortex dominated pressure distribution is visible at $\eta \leq 0.2$. The vortex induced features disappear at $\eta = 0.25$. At $\eta = 0.3$, the flow near the edge of the plate is influenced by the separation and the induced pressure distribution. A favorable pressure distribution is not created to delay the separation. Therefore, the edge configuration will play an important part in determining the induced pressure field. In Fig. 12 the skin friction at $\eta = 0.15$ does not indicate separation. As the ground height is increased, a recirculating region due to the separation is formed near the edge, and its extent increases accordingly.

Effect of Edge Configuration

Separation at the baffle plate edge is important in determining the induced pressure distribution on the lower surface

of the plate. The edge configuration, to a large extent, influences the separation.

A typical ground height studied here is $\eta = 0.25$. At this ground height, the standing vortex between the ground and the plate is still present, and the flow around the plate edge is about to separate. In Fig. 13, the skin friction coefficients for the three edge configurations are plotted together. The adverse pressure gradient towards the jet exit for the chamfered edge is severe enough to cause separation. Although the effect of the vortex is clearly visible, it is not able to suppress the separation. Both the rounded edge and the squared edge do not induce separation at this height. The different flow patterns around the plate edge subsequently influence the pressure distribution along the whole plate (Fig. 14). The chamfered edge induces the highest pressure loss. This observation correlates well with Corsiglia et al.[9] results, which are higher than others (Fig. 2). The squared edge and the rounded edge results differ only slightly. This feature is seen at all the ground heights studied. The comparatively small difference between the rounded and the squared edge configurations is perhaps not that surprising. It is possible that separation is induced at the first sharp edge of the squared edge plate, which alleviates the pressure loss. The resulting flow is similar to that due to the rounded edge.

The lift loss discrepancies between the three configurations are given in Fig. 15. The discrepancies are calculated based on the baseline configuration in terms of percentage. For the chamfered edge configuration, a 14% discrepancy is noted at around $\eta = 0.3$. As the ground height decreases, the discrepancy narrows. The reason was given in the previous sections as the appearance of the coherent vortex. As the ground height increases, the discrepancy between the squared edge and the chamfered edge remain largely constant at about 10%.

Effect of M_j and Turbulent Intensity

Computations were carried out at Mach 0.24, 0.35, 0.59, and 0.71 at $\eta = 0.3$. C_s was found to vary by only 0.5% over this subsonic range.

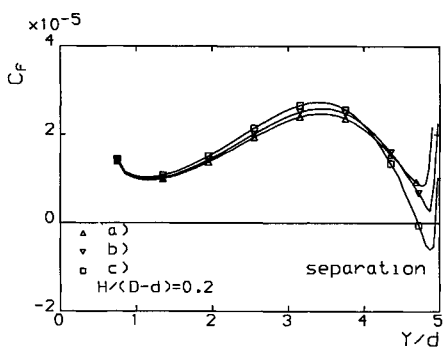

Fig. 13 Comparison between skin friction coefficients on the lower surface at $\eta = 0.2$: a) rounded edge, b) squared edge, and c) chamfered edge.

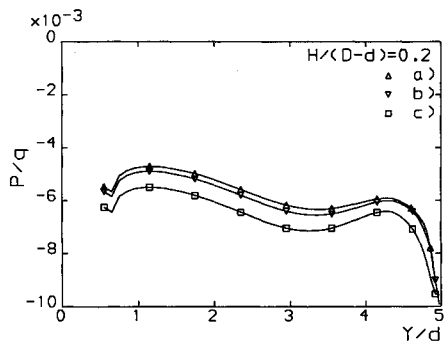

Fig. 14 Surface pressure on the lower surface at $\eta = 0.2$: a) rounded edge, b) squared edge, and c) chamfered edge.

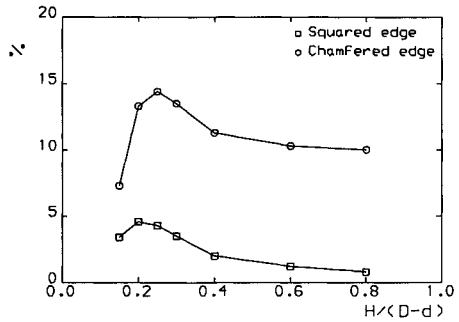

Fig. 15 Percentage lift loss discrepancies based on the rounded edge configuration.

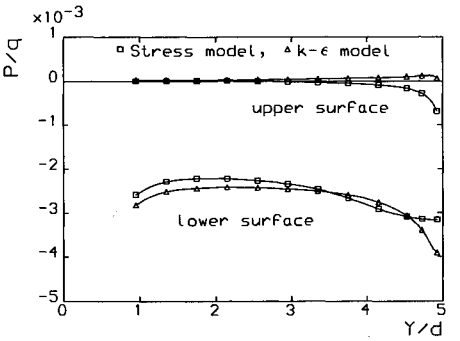

Fig. 16 Surface pressure comparison between the stress and the k-ε turbulence models at $\eta = 0.3$; square edge.

When the jet exit turbulent intensity was studied, k was varied between $0.002V_j^2$ and $0.1V_j^2$. The lift loss coefficient was found to reduce by approximately 4% between $0.002V_j^2 \leq k \leq 0.05V_j^2$, but was constant between $0.05V_j^2 < k \leq 0.1V_j^2$. This confirms the general belief that, in contrast to a free jet, wall jet entrainment is substantially invariant to changes in the exit turbulent level. The 4% reduction is due to the pressure drop near the jet exit. The contribution when integrated is relatively small.

Prediction at $\eta = 0.3$ with a Stress Model

The induced flowfield at $\eta = 0.3$ for the squared edge plate is calculated using a differential Reynolds stress model.[17] Comparison is made with the predictions given by the k-ε model. The overall flow features in terms of velocity, k, and streamline are similar. More importantly, the induced flow around the baffle plate also possesses similar features. There are, though, differences in the surface pressure distribution on the plate, which are shown in Fig. 16. The stress model is seen to give a slightly lower pressure suction near the jet exit. The difference, however, is relatively small. The pressure drop near the edge is smaller than that predicted with the k-ε model, the extent of which is increased. This type of pressure distribution was observed at higher ground heights when the k-ε model is used. Given the sensitivity of the pressure field to changes in the vortical field, this is perhaps not surprising. The predicted lift loss coefficient is about 11% smaller than that given by the k-ε model. This result is encouraging in that, if it is repeated over the whole ground height range, the overall agreement with the collected experimental data will improve significantly. The calculation with the stress model is not carried out further, as it is thought that it will not significantly enhance the quality of this particular study.

Summary

1) A coherent vortex exists beneath the outer portion of the baffle plate at low ground heights of $\eta < 0.25$. This vortex induces significant pressure drop on the lower surface of the baffle plate near the edge, and creates a favorable pressure

gradient to delay and/or even suppress the impending separation at the baffle plate edge.

2) At ground height $\eta \leq 0.2$, the outer boundary of the wall boundary layer attaches to the baffle plate.

3) At ground height $\eta \geq 0.25$, the induced flowfield between the ground and the baffle plate is dominated by the jet-induced entrainment and separation on the edge of the plate, which results in a recirculating region forming near the edge on the jet side of the plate, the extent of which increases with the ground height.

4) The chamfered edge induces the strongest separation at the edge of the plate, and subsequently the highest pressure loss on the lower surface. The rounded edge induces the weakest separation. The discrepancies between the chamfered edge and the rounded edge reaches 14% at $\eta = 0.3$. At $\eta \geq 0.3$, the discrepancy between the chamfered edge and the squared edge is largely constant at about 10%.

5) The differential Reynolds stress model is able to give a better prediction of the lift loss than the k-ε model.

Acknowledgments

The authors wish to thank the Nuffield Foundation for providing an award for the computational work and British Aerospace (Warton) for supporting part of the research.

References

[1]Wyatt, L. A., "Tests on the Loss of Vertical Jet Thrust Due to Ground Effect on Two Simple VTOL Platforms, with Particular Reference to the Short SCI Aircraft," Royal Aircraft Establishment, R&M 3313, London, May 1958.

[2]Spreemann, K. P., and Sherman, I. R., "Effects of Ground Proximity on the Thrust of a Simple Downward-Directed Jet Beneath a Flat Surface," NASA TN 4407, Sept. 1958.

[3]Davenport, E. E., and Spreemann, K. P., "Thrust Characteristics of Multiple Lifting Jets in Ground Proximity," NASA TN D-513, Sept. 1960.

[4]Wyatt, L. A., "Static Tests of Ground Effect on Planforms Fitted with a Centrally-Located Round Lifting Jet," Royal Aircraft Establishment, TN Aero. 2826, London, June 1962.

[5]Gentry, G. L., and Margason, R. J., "Jet-Induced Lift Losses on VTOL Configurations Hovering In and Out of Ground Effect," NASA TN D-3166, Feb. 1966.

[6]Hall, G. R., "Scaling of VTOL Aerodynamic Suckdown Forces," *Journal of Aircraft*, Vol. 4, No. 4, 1967, pp. 393, 394.

[7]Karemaa, A., Weber, H. A., Smith, C. W., and Garner, J. E., "The Aerodynamic and Thermodynamic Characteristics of Fountains and Some Far Field Temperature Distribution," General Dynamics Convair Div., Research Rept. ONR-CR212-237-1F, Aug. 1978.

[8]Christiansen, R. S., "A Large Scale Investigation of VSTOL Ground Effects," AIAA Paper 84-0336, Jan. 1984.

[9]Corsiglia, V. R., Wardwell, D. A., and Kuhn, R. E., "Small-Scale Experiments in STOVL Ground Effects," *Proceedings of International Power Lift Conference*, Royal Aeronautical Society, London, Aug. 1990, pp. III.14.1–III.14.13.

[10]Ing, D. N., and Bailey, P. J., "Correlation Between Wyatt and Other Studies on Single Jet In-Ground-Effect Lift Loss," Logico System Ltd. Rept. 24/1991, Surrey, England, UK, Jan. 1991.

[11]Oh, T. S., and Schetz, J. A., "Finite Element Simulation of Complex Jets in a Crossflow for V/STOL Applications," *AIAA Journal*, Vol. 27, No. 5, 1990, pp. 389–399.

[12]Chiu, S., Roth, K., and Margason, R., "A Numerical Investigation on a Subsonic Jet in a Crossflow," AIAA Paper 93-0870, 1993.

[13]Mayson, I., Ogilvie, F. B., and Harris, K. D., "An Investigation Under Static External Flow Conditions of the Axial Force Induced on Circular Flat Plates Surrounding Simple Uniform and Co-Axial Jets Exhausting Normally to the Plates," Hawker Siddeley Aviation, Research/1010/IM/FBO/KDH, UK, Dec. 1971.

[14]Lummus, J. R., "The Criticality of Engine Exhaust Simulations on VSTOL Model-measured Ground Effects," Office of Naval Research Rept. ONR-CR212-255-1F, Aug. 1979.

[15]Launder, B. E., and Spalding, D. B., "The Numerical Computation of Turbulent Flows," *Computational Methods in Applied Mechanical Engineering*, Vol. 3, No. 2, May 1974, pp. 269–289.

[16]Vasquez-Malebran, S., and Ing, D. N., "Navier-Stokes Simulation of a Single Impinging Jet Using the k-ε Model and a Specially Formulated Reynolds Stress/Algebraic Stress Model," Logico System Ltd. Rept. KRN-365, Surrey, England, UK, June 1985.

[17]Clarke, D. S., and Wilkes, N. S., "The Calculation of Turbulent Flows in Complex Geometries Using a Differential Stress Model," Harwell Lab. Rept. Atomic Energy Research Establishment Rept. 13428, Harwell, UK, 1989.

[18]Rhie, C. M., and Chow, W. L., "Numerical Study of the Turbulent Flow Past an Airfoil with Trailing Edge Separation," *AIAA Journal*, Vol. 21, No. 11, 1983, pp. 1527–1532.

[19]Van Doormaal, J. P., and Raithby, G. D., "Enhancement of the SIMPLE Method for Predicting Incompressible Fluid Flows," *Numerical Heat Transfer*, Vol. 7, April–June 1984, pp. 147–163.